INTERNATIONAL JOURNAL FOR NUMERICAL METHODS IN FLUIDS
Int. J. Numer. Meth. Fluids 2005; **48**:325–347
Published online 3 February 2005 in Wiley InterScience (www.interscience.wiley.com). DOI: 10.1002/fld.893

Stability/dispersion analysis of the discontinuous Galerkin linearized shallow-water system

Daniel Y. Le Roux[1,*,†] and G. F. Carey[2]

[1]*Département de Mathématiques et de Statistique, Université Laval, Québec, QC, Canada G1K 7P4*
[2]*Institute for Computational Engineering and Sciences, ASE/EM Department, The University of Texas at Austin, Austin, TX 78712, U.S.A.*

SUMMARY

The frequency or dispersion relation for the discontinuous Galerkin mixed formulation of the 1-D linearized shallow-water equations is analysed, using several basic DG mixed schemes. The dispersion properties are compared analytically and graphically with those of the mixed continuous Galerkin formulation for piecewise-linear bases on co-located grids. Unlike the Galerkin case, the DG scheme does not exhibit spurious stationary pressure modes. However, spurious propagating modes have been identified in all the present discontinuous Galerkin formulations. Numerical solutions of a test problem to simulate fast gravity modes illustrate the theoretical results and confirm the presence of spurious propagating modes in the DG schemes. Copyright © 2005 John Wiley & Sons, Ltd.

KEY WORDS: discontinuous Galerkin; finite elements; shallow-water equations; gravity waves

1. INTRODUCTION

Both mixed primitive variable and wave equation [1] forms of the shallow-water equations are extensively used in environmental studies and other applications. Finite-element continuous Galerkin (CG) techniques have gradually evolved to become the method of choice for this problem class [1–10]. This is largely because of the need to treat irregular boundary geometry in many applications. For example, both the coastal geometry and the bathymetry must be modeled adequately and hence calculations on graded meshes of unstructured grids are standard practice [11–17]. One of the issues associated with mixed formulations in general is the possibility of spurious modes that may arise for certain choices of bases. This difficulty

*Correspondence to: Daniel Y. Le Roux, Département de Mathématiques et de Statistique, Université Laval, Québec, QC, Canada G1K 7P4.
†E-mail: dleroux@mat.ulaval.ca

Contract/grant sponsor: Natural Sciences and Engineering Research (NSERC)
Contract/grant sponsor: Fonds Québecois de la Recherche sur la Nature et les Technologies (FQRNT)

Received 19 November 2003
Revised 16 November 2004
Accepted 19 November 2004

with mixed methods is not specific to the shallow-water problem alone but is well known also in other contexts such as primitive variable viscous flow where it has been extensively investigated for the CG mixed method [18–22]. However, the situation in the mixed shallow-water problem is different and, as noted initially in Reference [23] and in subsequent studies [5, 8, 17, 24], an analysis of the dispersion relation for a given formulation will explicitly ascertain the presence and determine the form of spurious modes as well as the dissipative/dispersive nature of a given formulation.

Discontinuous Galerkin (DG) schemes have been the focus of a number of recent studies in computational mechanics and computer codes are being developed for shallow-water applications using mixed formulation DG approaches [25–29]. A dispersion analysis of mixed DG formulations has not apparently been made previously and the purpose of the present work is to carry out such an analysis.

The examination of the spurious modes arising from mixed formulations has been focused almost exclusively on the spurious pressure or surface-elevation modes since these were argued to be the most troublesome [23]. These spurious modes are small-scale artifacts introduced by the spatial discretization scheme which do not propagate but are trapped within the model grid, and associated with zero frequency. If they are left undamped, they can cause an accumulation of energy in the smallest-resolvable scale, leading to noisy solutions.

The origin of the surface-elevation spurious modes is found in the coupling between the two operators that are responsible for rapidly propagating gravity waves in shallow-water models: the pressure gradient and divergence of velocity terms. Because these operators are linear, and the problems aforementioned occur in the context of linear formulations, solving *linear* equations is sufficient for our purpose. Further, the Coriolis operator will not be considered here because it is not concerned with the existence of surface-elevation spurious modes. Finally, as a foundation for understanding the behaviour and suitability of the DG mixed method in the context of shallow-water flows, one-dimensional equations will be considered. This permits constructive analysis to identify explicitly the asymptotic values of the discrete frequencies of each DG scheme and also allows a clear presentation of the propagating modes in numerical experiments.

Since the DG method introduces additional degrees of freedom for the same local choice of polynomial basis, it is intuitively reasonable that the richer subspace may admit more modes. In fact, we show that the DG scheme does not admit the usual stationary mode associated with the G scheme but instead the co-located DG schemes explored here generate fast spurious propagating modes. These modes propagating at three times the gravity mode speed, are high frequency but may be substantially damped as seen in the numerical experiments. This is the first study demonstrating this negative behaviour of mixed DG methods.

The paper is developed as follows: The one-dimensional shallow-water equations are considered in their simplest mixed velocity-elevation form for simplicity and convenience of subsequent constructions. Some basic DG formulations of this system are developed using different types of upwinding. We then consider the linear/linear co-located grid case, construct the associated dispersion relations and investigate spurious mode dependencies. The dispersion properties in each case are compared graphically with those of the standard mixed CG formulation. This stability/dispersion analysis is followed by numerical tests to demonstrate the presence and behaviour of fast propagating gravity modes. In the concluding remarks we summarize the results for these DG schemes and comment on other related schemes.

2. MODEL PROBLEM AND MODAL BEHAVIOUR

For an enclosed domain of length L, where $0<x<L$, the one-dimensional, inviscid, linearized form of the shallow-water equations may be expressed in Cartesian coordinates [30] as

$$u_t + g\eta_x = 0 \tag{1}$$

$$\eta_t + Hu_x = 0 \tag{2}$$

where u is the velocity variable, η is the surface elevation with respect to the reference level $z=0$, g is the gravitational acceleration and the mean depth H is assumed constant. Boundary and initial data complete the specification of the problem.

A linear stability analysis of (1) and (2) reveals that there is one basic kind of associated motion, small-amplitude fast-moving gravitational oscillations. Indeed, if we examine the free modes of (1) and (2) by perturbing about the basic state $u=\eta=0$, and substituting periodic solutions of the form $u=\tilde{u}e^{i(kx+\omega t)}$ and $\eta=\tilde{\eta}e^{i(kx+\omega t)}$ into (1) and (2), where $\tilde{u}$ and $\tilde{\eta}$ are amplitudes, k is the wave number in the x-direction and ω is the angular frequency, we may then obtain an equation for the frequency by noting that the determinant of the coefficients must be zero for a nontrivial solution. The resulting frequency equation is then

$$\omega^2 - gHk^2 = 0 \tag{3}$$

The two solutions $\omega=\pm\sqrt{gH}k$, correspond to the free-surface gravitational modes. The gravity waves can propagate along the $-x$ axis in both directions at a speed $\omega/k=\sqrt{gH}$, independently of the wave number k, and hence there is no dispersion of the waves.

We now illustrate the possible occurrence of stationary surface-elevation spurious modes in the discretization of (1) and (2). Consider a uniform mesh of m intervals on $(0,L)$ and let $h=L/m$ denote the meshlength parameter with nodes $x_j=(j-1)h$ for $j=1,2,\ldots,m+1$. By semi-discretizing (1) and (2) in space and approximating the derivatives using centered finite differences at nodes $j=1,2,3,\ldots$, we obtain

$$\frac{\partial u_j}{\partial t} + g\,\frac{\eta_{j+1}-\eta_{j-1}}{2h} = 0 \tag{4}$$

$$\frac{\partial \eta_j}{\partial t} + H\,\frac{u_{j+1}-u_{j-1}}{2h} = 0 \tag{5}$$

where u_j and η_j, $j=1,2,3,\ldots$, are located at the same nodal positions (co-located), as shown in Figure 1.

By substituting $u_j=\tilde{u}e^{i(kx_j+\omega t)}$ and $\eta_j=\tilde{\eta}e^{i(kx_j+\omega t)}$ into (4) and (5), we obtain

$$\begin{pmatrix} \omega & g\,\dfrac{\sin kh}{h} \\ H\,\dfrac{\sin kh}{h} & \omega \end{pmatrix} \begin{pmatrix} \tilde{u} \\ \tilde{\eta} \end{pmatrix} = \begin{pmatrix} 0 \\ 0 \end{pmatrix} \tag{6}$$

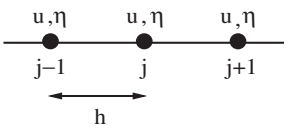

Figure 1. The variables u and η are located at the same nodal positions.

and the resulting frequency equation is

$$\omega = \sqrt{gH}\,\frac{\sin\, kh}{h} \tag{7}$$

Now the phase speed is a function of k and $\omega/k = 0$ for $kh = \pi$. Note in the CG case, the same reasoning would also lead to the factor sin kh in the corresponding frequency equation. Hence, the wave with wave length $2h$ is stationary and trapped within the mesh. It corresponds to a physical eigenmode of the system which has its phase speed reduced to zero by the numerical method and appears as a stationary spurious oscillation [23] with $\eta_j = (-1)^j$ and $u_j = 0,\ j = 1, 2, 3, \ldots$. The second solution where $\omega = 0$ corresponds to $k = 0$ so that $\eta_j = 1$, $j = 1, 2, 3, \ldots$. It is the hydrostatic mode and can be simply considered as a constant of integration associated with the solution of the governing equations. In the following section we briefly discuss the effect of time discretization and then focus on the main topic of this study—propagating modes of the DG scheme.

3. TEMPORAL DISCRETIZATION

Rapidly propagating gravitational disturbances usually carry relatively little energy for many geophysical flows when compared to the modes of the large-scale dynamics. However, they considerably limit the maximum timestep allowed by the CFL stability criterion in formulations that use an explicit time discretization. In an atmospheric context, Robert *et al.* [31, 32] demonstrated that much larger timesteps can be used if the linear terms responsible for the rapidly propagating gravitational oscillations are treated semi-implicitly, *via* a trapezoidal Crank–Nicolson scheme. The semi-implicit scheme dramatically reduces the phase speeds of these fast disturbances without modifying their amplitude, and it has a negligible impact on the large- and 'synoptic'-scale dynamics. Hence, the Crank–Nicolson scheme will be of interest for many applications, unless an accurate representation of the fast gravity modes is important. Further, the use of a purely implicit scheme, although quite stable, is only first order accurate and would thus severely damp the amplitude of the fast gravity waves.

For a given time step $\Delta t = t^{n+1} - t^n$ we introduce a general 2-level time discretization of (1) and (2) of the form

$$u^{n+1} + \sigma g \Delta t \eta_x^{n+1} = u^n - (1-\sigma) g \Delta t \eta_x^n \tag{8}$$

$$\eta^{n+1} + \sigma H \Delta t u_x^{n+1} = \eta^n - (1-\sigma) H \Delta t u_x^n \tag{9}$$

where σ is a real parameter such that $0 \leqslant \sigma \leqslant 1$. Observe that the standard choices $\sigma = 0, \frac{1}{2}, 1$ yield the respective forward Euler, trapezoidal Crank–Nicolson and backward Euler type

schemes. Other choices such as Runge Kutta schemes are possible, but they would make the present stability/dispersion analysis much less tractable.

Equations (8) and (9) are now spatially discretized using the DG method.

4. DISCONTINUOUS GALERKIN FORMULATION

Let ε_h denote a partition of the model domain $\Omega=(0,L)$, i.e. ε_h is a finite collection of m open elements e_j, $j=1,2,\ldots,m$, of the real line, such that

$$\bar{\Omega}=\bigcup_{e_j\in\varepsilon_h}\bar{e}_j \quad \text{and} \quad e_i\cap e_j=\emptyset \text{ for } i\neq j$$

Consider a uniform mesh of m intervals on $(0,L)$ and let $h=L/m$ denote the meshlength parameter with elements $e_j=(x_j,x_{j+1})$ for $j=1,2,\ldots,m$ and nodes $x_j=(j-1)h$ for $j=1,2,\ldots,m+1$. For any given open set ϖ (ϖ may define the whole domain Ω, or an element e_j, $j=1,2,\ldots,m$, of ε_h), the space $H^1(\varpi)$ will denote the usual Sobolev space of functions in the square-integrable space $L^2(\varpi)$, whose first derivatives belong to $L^2(\varpi)$. The so-called (mesh-dependent) *broken space* $H^1(\varepsilon_h)$ will be defined as

$$H^1(\varepsilon_h)=\{v\in L^2(\Omega);\ v|_e\in H^1(e),\ \forall e\in\varepsilon_h\}$$

where e simply denotes an element e_j, $j=1,2,\ldots,m$, of ε_h.

Let u and η be sufficiently smooth functions, whose regularity will be examined later. Multiplying (8) and (9) by functions φ and ψ, respectively, belonging to $H^1(\varepsilon_h)$, and integrating over the domain Ω we obtain: find u^{n+1} and η^{n+1} satisfying the essential boundary conditions and such that the following holds for each timestep Δt:

$$\int_\Omega u^{n+1}\varphi\,\mathrm{d}x+\sigma g\Delta t\int_\Omega \eta_x^{n+1}\varphi\,\mathrm{d}x=\int_\Omega u^n\varphi\,\mathrm{d}x-(1-\sigma)g\Delta t\int_\Omega \eta_x^n\varphi\,\mathrm{d}x \tag{10}$$

$$\int_\Omega \eta^{n+1}\psi\,\mathrm{d}x+\sigma H\Delta t\int_\Omega u_x^{n+1}\psi\,\mathrm{d}x=\int_\Omega \eta^n\psi\,\mathrm{d}x-(1-\sigma)H\Delta t\int_\Omega u_x^n\psi\,\mathrm{d}x \tag{11}$$

To obtain the DG formulation we proceed as follows: first, decompose the integrals in (10) and (11) into element contributions and integrate by parts, yielding

$$\sum_{j=1}^m\int_{e_j}u^{n+1}\varphi\,\mathrm{d}x-\sigma g\Delta t\sum_{j=1}^m\left(\int_{e_j}\eta^{n+1}\varphi_x\,\mathrm{d}x-\eta^{n+1}\varphi\,|_{j^+}^{(j+1)^-}\right)$$

$$=\sum_{j=1}^m\int_{e_j}u^n\varphi\,\mathrm{d}x+(1-\sigma)g\Delta t\sum_{j=1}^m\left(\int_{e_j}\eta^n\varphi_x\,\mathrm{d}x-\eta^n\varphi\,|_{j^+}^{(j+1)^-}\right) \tag{12}$$

$$\sum_{j=1}^m\int_{e_j}\eta^{n+1}\psi\,\mathrm{d}x-\sigma H\Delta t\sum_{j=1}^m\left(\int_{e_j}u^{n+1}\psi_x\,\mathrm{d}x-u^{n+1}\psi\,|_{j^+}^{(j+1)^-}\right)$$

$$=\sum_{j=1}^m\int_{e_j}\eta^n\psi\,\mathrm{d}x+(1-\sigma)H\Delta t\sum_{j=1}^m\left(\int_{e_j}u^n\psi_x\,\mathrm{d}x-u^n\psi\,|_{j^+}^{(j+1)^-}\right) \tag{13}$$

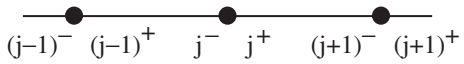

Figure 2. Node j corresponds to the coincident node pair (j^-/j^+), $j=2,3,\ldots,m$.

with j^- and j^+ being the nodal positions of adjacent elements corresponding to a typical node j. That is, for interior nodes, j corresponds to the coincident node pair (j^-/j^+), $j=2,3,\ldots,m$, as shown in Figure 2.

At time t^n (and also at time t^{n+1} by replacing n by $n+1$) we regroup terms to write

$$\sum_{j=1}^{m} \eta^n \varphi \,|_{j^+}^{(j+1)^-} = \sum_{j=1}^{m+1} (\eta_{j^-}^n \varphi_{j^-} - \eta_{j^+}^n \varphi_{j^+}) \tag{14}$$

$$\sum_{j=1}^{m} u^n \psi \,|_{j^+}^{(j+1)^-} = \sum_{j=1}^{m+1} (u_{j^-}^n \psi_{j^-} - u_{j^+}^n \psi_{j^+}) \tag{15}$$

with $u=\eta=0$ at nodes 1^- and $(m+1)^+$.

Next, introduce

$$\langle \chi_j \rangle_\lambda = (1-\lambda)\chi_{j^-} + \lambda \chi_{j^+} \quad \text{and} \quad [\chi_j] = \chi_{j^-} - \chi_{j^+} \tag{16}$$

as the weighted averages and jump of χ, respectively, at node j for $j=1,2,\ldots,m+1$.

Using the formula

$$ab - cd = ((1-\lambda)a + \lambda c)(b-d) + (a-c)(\lambda b + (1-\lambda)d) \tag{17}$$

$$= (\lambda a + (1-\lambda)c)(b-d) + (a-c)((1-\lambda)b + \lambda d) \tag{18}$$

where a,b,c,d are real numbers and λ is a real parameter, equations (14) and (15) can be conveniently expressed as

$$\sum_{j=1}^{m} \eta^n \varphi \,|_{j^+}^{(j+1)^-} = \sum_{j=1}^{m+1} (\langle \eta_j^n \rangle_\mu [\varphi_j] + [\eta_j] \langle \varphi_j^n \rangle_{1-\mu}) \tag{19}$$

$$\sum_{j=1}^{m} u^n \psi \,|_{j^+}^{(j+1)^-} = \sum_{j=1}^{m+1} (\langle u_j^n \rangle_\nu [\psi_j] + [u_j] \langle \psi_j^n \rangle_{1-\nu}) \tag{20}$$

where $(\mu,\nu)=(\lambda,\lambda)$ or $(\mu,\nu)=(\lambda,1-\lambda)$ or $(\mu,\nu)=(1-\lambda,\lambda)$. The case $\lambda=\frac{1}{2}$ obviously leads to the same results.

When u and η belong to $H^1(\Omega) \subset H^1(\varepsilon_h)$ the jumps $[u_j]$ and $[\eta_j]$ vanish on each 'knot' x_j, $j=1,2,\ldots,m+1$, so that (19) and (20) become

$$\sum_{j=1}^{m} \eta^n \varphi \,|_{j^+}^{(j+1)^-} = \sum_{j=1}^{m+1} \langle \eta_j^n \rangle_\mu [\varphi_j] \tag{21}$$

$$\sum_{j=1}^{m} u^n \psi \,|_{j^+}^{(j+1)^-} = \sum_{j=1}^{m+1} \langle u_j^n \rangle_\nu [\psi_j] \tag{22}$$

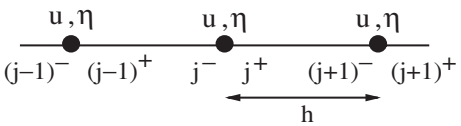

Figure 3. Position of the variables u and η on the grid.

Equations (21) and (22) are then used in (12)–(13) to obtain the desired form of the weak formulation.

In the DG approximation, we consider finite element spaces V_h^k of polynomial functions, discontinuous at the element interfaces, such that

$$V_h^k = \{v_h \in L^2(\Omega);\ v_h|_e = \hat{v}_h \circ F_e^{-1},\ \hat{v}_h \in P_k(\hat{e}),\ \forall\, e \in \varepsilon_h\}$$

where F_e is the affine mapping from the master element $\hat{e}$ to the element e in the partition, and $P_k(\hat{e})$ is the space of polynomial functions of degree at most k on $\hat{e}$.

Introducing the finite-element basis leads to a finite-element discretization that consists in finding u_h and η_h belonging to V_h^k for the selected meshes and bases, such that

$$\sum_{j=1}^{m} \int_{e_j} u_h^{n+1} \varphi \,\mathrm{d}x - \sigma g \Delta t \sum_{j=1}^{m} \left(\int_{e_j} \eta_h^{n+1} \varphi_x \,\mathrm{d}x - \langle \eta_j^{n+1} \rangle_\mu [\varphi_j] \right)$$
$$= \sum_{j=1}^{m} \int_{e_j} u_h^n \varphi \,\mathrm{d}x + (1-\sigma) g \Delta t \sum_{j=1}^{m} \left(\int_{e_j} \eta_h^n \varphi_x \,\mathrm{d}x - \langle \eta_j^n \rangle_\mu [\varphi_j] \right) \tag{23}$$

$$\sum_{j=1}^{m} \int_{e_j} \eta_h^{n+1} \psi \,\mathrm{d}x - \sigma H \Delta t \sum_{j=1}^{m} \left(\int_{e_j} u_h^{n+1} \psi_x \,\mathrm{d}x - \langle u_j^{n+1} \rangle_\nu [\psi_j] \right)$$
$$= \sum_{j=1}^{m} \int_{e_j} \eta_h^n \psi \,\mathrm{d}x + (1-\sigma) H \Delta t \sum_{j=1}^{m} \left(\int_{e_j} u_h^n \psi_x \,\mathrm{d}x - \langle u_j^n \rangle_\nu [\psi_j] \right) \tag{24}$$

In the present study, the velocity and surface elevation fields are discretized by using the same piecewise-linear basis functions and the variables for discontinuous u_h and η_h are located at the same nodal positions x_j ($j = 1, 2, \ldots, m+1$), with $h = L/m$ the nodal spacing, as shown in Figure 3.

Other possible choices of bases may be considered, for example high-order basis functions, but those investigated here are of most practical interest. Indeed, as previously mentioned, unless an accurate representation of the rapidly propagating gravitational oscillations is desired, a Crank–Nicolson time stepping scheme may be efficiently used to treat the linear terms responsible for their propagation. Consequently, the phase speed of these fast waves (not their amplitude) is greatly retarded by the semi-implicit scheme and a high-order spatial discretization of the terms that govern their propagation is therefore not warranted. This is true for many applications where the rapid gravitational oscillations carry negligible energy. In the next section we present the main analytical results of the present work concerning propagating spurious modes.

5. STABILITY/DISPERSION ANALYSIS

A stability/dispersion analysis is now constructed for the DG schemes based on three different choices for representing the fluxes at the element interfaces.

5.1. *The case* $\mu = v = \lambda$ (DG1)

Equation (23) at node j^+ for $\varphi = \varphi_{j^+}$ becomes

$$\int_{e_j} (u_{j^+}^{n+1}\varphi_{j^+} + u_{(j+1)^-}^{n+1}\varphi_{(j+1)^-})\varphi_{j^+}\,\mathrm{d}x - \sigma g\Delta t \int_{e_j} (\eta_{j^+}^{n+1}\varphi_{j^+} + \eta_{(j+1)^-}^{n+1}\varphi_{(j+1)^-})(\varphi_{j^+})_x\,\mathrm{d}x$$
$$+\sigma g\Delta t(\langle\eta_j^{n+1}\rangle_\lambda[\varphi_j] + \langle\eta_{j+1}^{n+1}\rangle_\lambda[\varphi_{(j+1)}])$$
$$= \int_{e_j} (u_{j^+}^{n}\varphi_{j^+} + u_{(j+1)^-}^{n}\varphi_{(j+1)^-})\varphi_{j^+}\,\mathrm{d}x + (1-\sigma)g\Delta t \int_{e_j} (\eta_{j^+}^{n}\varphi_{j^+} + \eta_{(j+1)^-}^{n}\varphi_{(j+1)^-})(\varphi_{j^+})_x\,\mathrm{d}x$$
$$-(1-\sigma)g\Delta t(\langle\eta_j^{n}\rangle_\lambda[\varphi_j] + \langle\eta_{j+1}^{n}\rangle_\lambda[\varphi_{(j+1)}]) \tag{25}$$

where u_h and η_h have been expanded over element e_j, at times t^{n+1} and t^n, in terms of their nodal values for the element, using the basis functions φ_{j^+} and $\varphi_{(j+1)^-}$. Since the latter are linear over element e_j, we have $\varphi_{j^+} = (x - x_{j+1})/(x_j - x_{j+1})$ and $\varphi_{(j+1)^-} = (x - x_j)/(x_{j+1} - x_j)$. We then deduce $[\varphi_j] = \varphi_{j^-} - \varphi_{j^+} = -1$ and $[\varphi_{(j+1)}] = 0$ at node j^+, $(\varphi_{j^+})_x = -1/h$, and

$$\int_{e_j} \varphi_{j^+}\varphi_{j^+}\,\mathrm{d}x = \frac{h}{3}, \quad \int_{e_j} \varphi_{j^+}\varphi_{(j+1)^-}\,\mathrm{d}x = \frac{h}{6}, \quad \int_{e_j} \varphi_{j^+}\,\mathrm{d}x = \int_{e_j} \varphi_{(j+1)^-}\,\mathrm{d}x = \frac{h}{2}$$

By using (16) we finally obtain

$$\frac{h}{3}u_{j^+}^{n+1} + \frac{h}{6}u_{(j+1)^-}^{n+1} + \frac{\sigma}{2}g\Delta t(2(\lambda-1)\eta_{j^-}^{n+1} + (1-2\lambda)\eta_{j^+}^{n+1} + \eta_{(j+1)^-}^{n+1})$$
$$= \frac{h}{3}u_{j^+}^{n} + \frac{h}{6}u_{(j+1)^-}^{n} - \frac{(1-\sigma)}{2}g\Delta t(2(\lambda-1)\eta_{j^-}^{n} + (1-2\lambda)\eta_{j^+}^{n} + \eta_{(j+1)^-}^{n}) \tag{26}$$

Equation (23) at node $(j+1)^-$ for $\varphi = \varphi_{(j+1)^-}$, and following the same procedure, leads to

$$\frac{h}{6}u_{j^+}^{n+1} + \frac{h}{3}u_{(j+1)^-}^{n+1} + \frac{\sigma}{2}g\Delta t(-\eta_{j^+}^{n+1} + (1-2\lambda)\eta_{(j+1)^-}^{n+1} + 2\lambda\eta_{(j+1)^+}^{n+1})$$
$$= \frac{h}{6}u_{j^+}^{n} + \frac{h}{3}u_{(j+1)^-}^{n} - \frac{(1-\sigma)}{2}g\Delta t(-\eta_{j^+}^{n} + (1-2\lambda)\eta_{(j+1)^-}^{n} + 2\lambda\eta_{(j+1)^+}^{n}) \tag{27}$$

Similarly, for (24) with $\psi = \psi_{j^+}$ and $\psi = \psi_{(j+1)^-}$ respectively

$$\frac{h}{3}\eta_{j^+}^{n+1} + \frac{h}{6}\eta_{(j+1)^-}^{n+1} + \frac{\sigma}{2}H\Delta t(2(\lambda-1)u_{j^-}^{n+1} + (1-2\lambda)u_{j^+}^{n+1} + u_{(j+1)^-}^{n+1})$$
$$= \frac{h}{3}\eta_{j^+}^{n} + \frac{h}{6}\eta_{(j+1)^-}^{n} - \frac{(1-\sigma)}{2}H\Delta t(2(\lambda-1)u_{j^-}^{n} + (1-2\lambda)u_{j^+}^{n} + u_{(j+1)^-}^{n}) \tag{28}$$

$$\frac{h}{6}\eta_{j^+}^{n+1}+\frac{h}{3}\eta_{(j+1)^-}^{n+1}+\frac{\sigma}{2}H\Delta t(-u_{j^+}^{n+1}+(1-2\lambda)u_{(j+1)^-}^{n+1}+2\lambda u_{(j+1)^+}^{n+1})$$
$$=\frac{h}{6}\eta_{j^+}^{n}+\frac{h}{3}\eta_{(j+1)^-}^{n}-\frac{(1-\sigma)}{2}H\Delta t(-u_{j^+}^{n}+(1-2\lambda)u_{(j+1)^-}^{n}+2\lambda u_{(j+1)^+}^{n}) \tag{29}$$

Periodic solutions of discrete system (26)–(29) corresponding to $u_{j\pm}=\tilde{u}_{\pm}\mathrm{e}^{\mathrm{i}(kx_{j\pm}+\omega t)}$ and $\eta_{j\pm}=\tilde{\eta}_{\pm}\mathrm{e}^{\mathrm{i}(kx_{j\pm}+\omega t)}$ are sought. Substituting in (26)–(29) and setting

$$E=\mathrm{e}^{\mathrm{i}\omega\Delta t},\quad \alpha=\frac{h}{6}(E-1),\quad \beta=\frac{\Delta t}{2}([E-1]\sigma+1) \tag{30}$$

to simplify the resulting relations, we obtain

$$\begin{pmatrix} 2\alpha & \alpha\mathrm{e}^{\mathrm{i}kh} & g\beta(1-2\lambda) & g\beta(\mathrm{e}^{\mathrm{i}kh}-2+2\lambda)\\ \alpha\mathrm{e}^{-\mathrm{i}kh} & 2\alpha & g\beta(2\lambda-\mathrm{e}^{-\mathrm{i}kh}) & g\beta(1-2\lambda)\\ H\beta(1-2\lambda) & H\beta(\mathrm{e}^{\mathrm{i}kh}-2+2\lambda) & 2\alpha & \alpha\mathrm{e}^{\mathrm{i}kh}\\ H\beta(2\lambda-\mathrm{e}^{-\mathrm{i}kh}) & H\beta(1-2\lambda) & \alpha\mathrm{e}^{-\mathrm{i}kh} & 2\alpha \end{pmatrix}\mathbf{X}=\mathbf{0} \tag{31}$$

where $\mathbf{X}^{\mathrm{t}}=(\tilde{u}_+,\tilde{u}_-,\tilde{\eta}_+,\tilde{\eta}_-)$ and $\mathbf{0}^{\mathrm{t}}=(0,0,0,0)$.

For a non-trivial solution $\mathbf{X}$ to exist, the determinant of the matrix in the left hand side of (31) must vanish. This condition implies

$$9\alpha^4+4gH\alpha^2\beta^2A+4g^2H^2\beta^4B=0 \tag{32}$$

with

$$A=-1+18\lambda-18\lambda^2+\mathrm{e}^{-\mathrm{i}kh}(7[2\lambda-1]+\lambda-8\lambda^2)+\mathrm{e}^{\mathrm{i}kh}(\lambda-8\lambda^2)$$
$$+\mathrm{e}^{-2\mathrm{i}kh}(2\lambda-1-\lambda^2)+\mathrm{e}^{2\mathrm{i}kh}(-\lambda^2) \tag{33}$$

$$B=1+2\lambda-2\lambda^2+\mathrm{e}^{-\mathrm{i}kh}(2[2\lambda-1]-2\lambda)+\mathrm{e}^{\mathrm{i}kh}(-2\lambda)$$
$$+\mathrm{e}^{-2\mathrm{i}kh}(1-2\lambda+\lambda^2)+\mathrm{e}^{2\mathrm{i}kh}(\lambda^2) \tag{34}$$

Solving (32) for α^2 and using (30) we obtain the following pair of solutions for E:

$$E_j^{\pm}=\frac{1\pm(1-\sigma)c(r_j^{\mathrm{R}}+\mathrm{i}r_j^{\mathrm{I}})}{1\mp\sigma c(r_j^{\mathrm{R}}+\mathrm{i}r_j^{\mathrm{I}})},\quad j=1,2 \tag{35}$$

where $c\equiv\sqrt{gH}\Delta t/h$ is the gravitational Courant number and

$$r_j=\sqrt{-2A\pm2\sqrt{A^2-9B}}\equiv r_j^{\mathrm{R}}+\mathrm{i}r_j^{\mathrm{I}},\quad j=1,2 \tag{36}$$

where r_j^{R} and r_j^{I} are respectively the real and imaginary parts of r_j, $j=1,2$.

In the limit as infinitesimal time step $\Delta t\to0$ and for all σ, the discrete frequencies obtained from (35) asymptote to the complex expressions

$$\omega_j=\pm\frac{\sqrt{gH}}{h}(r_j^{\mathrm{I}}-\mathrm{i}r_j^{\mathrm{R}}),\quad j=1,2 \tag{37}$$

and for infinitesimal mesh spacing we obtain

$$\omega_1 = \begin{cases} \pm\sqrt{gH}\,\mathrm{sgn}\left(\lambda-\frac{1}{2}\right)\left(-\mathrm{i}\,\frac{6(2\lambda-1)}{h}+3k+\mathrm{i}(2\lambda-1)k^2h-\frac{1}{3}k^3h^2+O(h^3)\right) \\ \text{if} \quad \lambda\neq\frac{1}{2}, \\ \pm\sqrt{gH}\left(k+\frac{1}{48}k^3h^2+O(h^4)\right) \quad \text{if} \quad \lambda=\frac{1}{2} \end{cases} \tag{38}$$

$$\omega_2 = \begin{cases} \pm\sqrt{gH}\left(k+\mathrm{i}\,\frac{1}{72(2\lambda-1)}k^4h^3+O(h^4)\right) \quad \text{if} \quad \lambda\neq\frac{1}{2} \\ \pm\sqrt{gH}\left(3k-\frac{5}{16}k^3h^2+O(h^4)\right) \quad \text{if} \quad \lambda=\frac{1}{2} \end{cases} \tag{39}$$

Note that ω_1 in (38) and ω_2 in (39) coincide with the continuous solution obtained from (3) in the limit as mesh spacing $h\to 0$ only when $\lambda=\frac{1}{2}$ in (38) and $\lambda\neq\frac{1}{2}$ in (39), respectively. For $\lambda\neq\frac{1}{2}$ in (38) and $\lambda=\frac{1}{2}$ in (39), ω_1 and ω_2, respectively, correspond to spurious *propagating* modes from the DG scheme.

Equation (35) leads to

$$|E_j^{\pm}| = \sqrt{\frac{(1\pm[1-\sigma]cr_j^{\mathrm{R}})^2+([1-\sigma]cr_j^{\mathrm{I}})^2}{(1\mp\sigma cr_j^{\mathrm{R}})^2+(\sigma cr_j^{\mathrm{I}})^2}} \quad j=1,2 \tag{40}$$

A necessary and sufficient condition for stability is then obtained from (40)

$$|E_j^{\pm}|\leqslant 1 \iff c(2\sigma-1)((r_j^{\mathrm{R}})^2+(r_j^{\mathrm{I}})^2)\geqslant \pm 2r_j^{\mathrm{R}}, \quad j=1,2 \tag{41}$$

In the present instance the results are compared with those of the CG case, which is denoted by $|E_*|$, with

$$|E_*| = \sqrt{\frac{1+(1-\sigma)^2c^2r_*^2}{1+\sigma^2c^2r_*^2}} \quad \text{where} \quad r_* = \frac{3\sin kh}{2+\cos kh} \tag{42}$$

The values of $|E_j^{\pm}|$, $j=1,2$, are plotted in Figure 4 as a function of c and kh for $\sigma=\frac{1}{2}$ and $\sigma=1$, in the cases $\lambda=0$ and $\frac{1}{4}$, and in Figure 5 for $\sigma=1$ in the case $\lambda=\frac{1}{2}$. In the following numerical results (e.g. see Figure 4) we test for $\lambda=0,\frac{1}{4},\frac{1}{2}$. Note that $E_j(\lambda)=E_j(1-\lambda)$, so the results are symmetric with respect to choice of λ in this sense. That is, $E_j(\frac{1}{4})=E_j(\frac{3}{4})$. Returning to Figure 4, $|E_1^+|$ tends to infinity for $k=0$ and $c=\frac{1}{3}$ and $\frac{2}{3}$ in the case $\sigma=\frac{1}{2}$ with $\lambda=0$ and $\frac{1}{4}$, respectively, and $c=\frac{1}{6}$ and $\frac{1}{3}$ in the case $\sigma=1$ with $\lambda=0$ and $\frac{1}{4}$, respectively. This behaviour is presumably due to the term $-\mathrm{i}6(2\lambda-1)/h$ in (38) for $\lambda\neq\frac{1}{2}$, a source of potential instability. In fact, the present scheme will become unstable as soon as $\lambda\neq\frac{1}{2}$. The term $-\mathrm{i}6(2\lambda-1)/h$ in (38) is also responsible for the strange behaviour of $|E_1^-|$ in Figure 4 for $k=0$, since $|E_1^-|\neq 1$ except when $c=0$, and $|E_1^-|=0$ for $c=\frac{1}{3}$ (case $\lambda=0$) and $c=\frac{2}{3}$ (case $\lambda=\frac{1}{4}$). It is also observed, in Figure 4, that for $\sigma=\frac{1}{2}$ $|E_2^+|$ is greater than 1 for some values of kh.

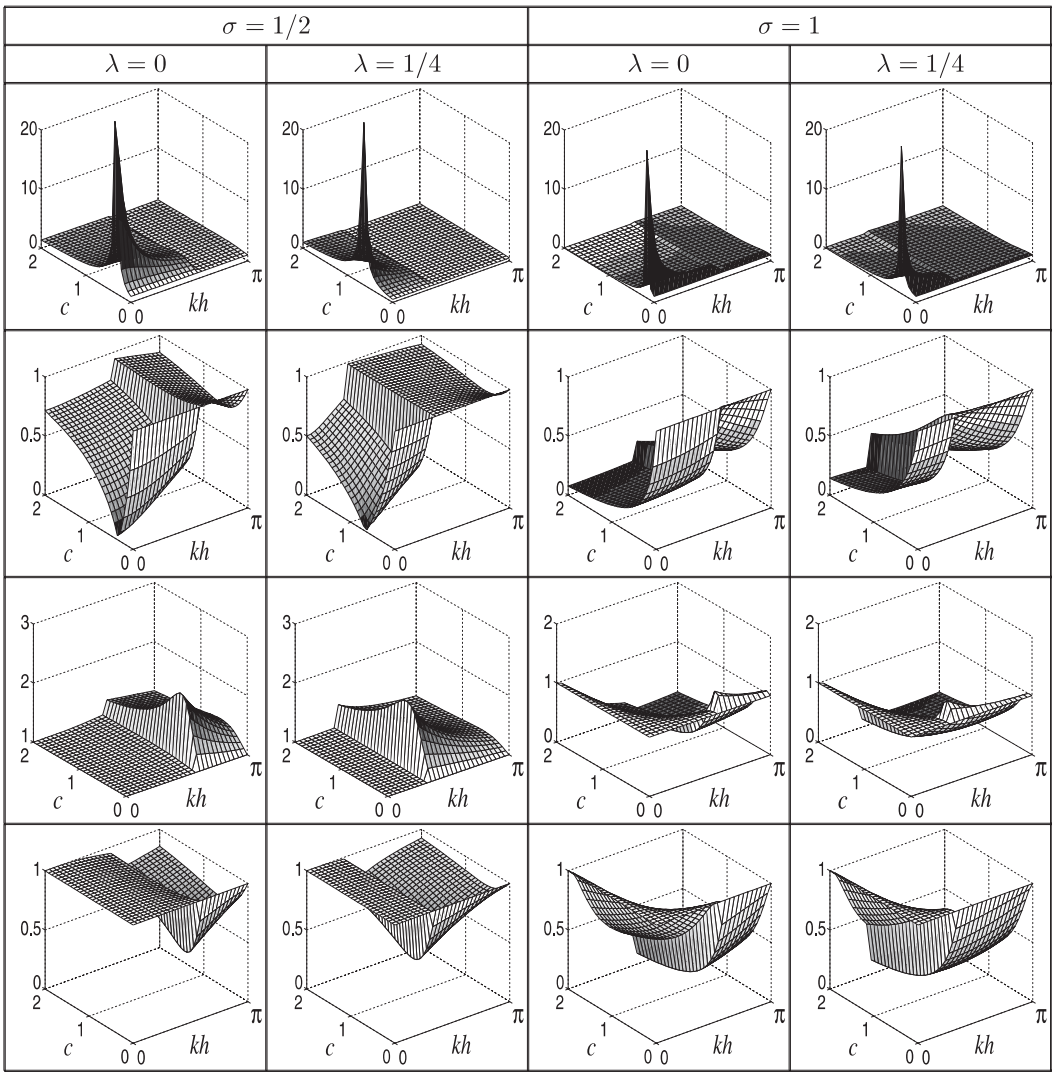

Figure 4. $|E_j^{\pm}|$, $j=1,2$, in the cases $\sigma=\frac{1}{2}$ and 1, with $\lambda=0$ and $\frac{1}{4}$. The lines 1, 2, 3 and 4 correspond to $|E_1^+|, |E_1^-|, |E_2^+|$ and $|E_2^-|$, respectively.

Some damping of the solution occurs in the case $\sigma=1$, as shown in Figure 4 (except for $|E_1^+|$). Similar damping occurs for $\lambda=\frac{1}{2}$, as seen in Figure 5, and it is compared with the damping in the CG scheme. The results obtained for $\sigma=\frac{1}{2}$ in Figure 4 are somewhat surprising since some damping is observed for $|E_1^-|$ and $|E_2^-|$. However, from (41) and for $\sigma=\frac{1}{2}$, we deduce the scheme is neutrally stable ($|E_j^{\pm}|=1$) only if $r_j^{\mathrm{R}}=0$, $j=1,2$, contrary to the CG case. It is observed graphically that $r_j^{\mathrm{R}}=0$, $j=1,2$, when $\lambda=\frac{1}{2}$ only. This particular choice of λ leads to real expressions for A and B in (33) and (34), respectively, with

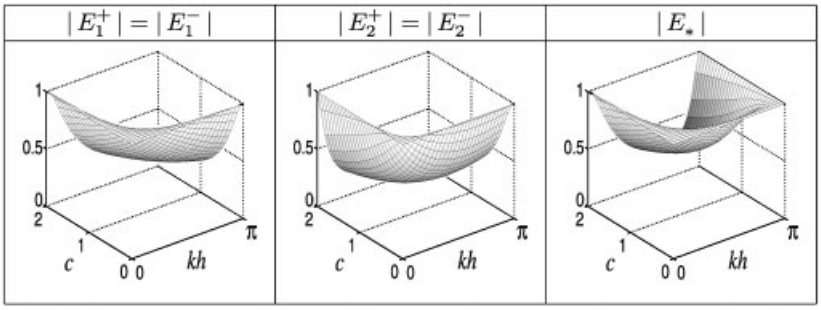

Figure 5. $|E_j^{\pm}|$, $j=1,2$, and $|E_*|$ in the case $\sigma=1$ with $\lambda=\frac{1}{2}$.

$-2A \pm 2\sqrt{A^2-9B} < 0$, and hence to $r_j^{\mathrm{R}} = 0$ and $r_j^{\mathrm{I}} = \sqrt{2A \mp 2\sqrt{A^2-9B}}$, $j=1,2$, or

$$r_j^{\mathrm{I}} = 2\left|\sin\frac{kh}{2}\right|\sqrt{4+\cos kh \pm \sqrt{(4+\cos kh)^2-9}} \tag{43}$$

with $1 \leqslant 4+\cos kh - \sqrt{(4+\cos kh)^2-9} \leqslant 3$ for all kh. Hence, for $\sigma=\frac{1}{2}$, $|E_j^{\pm}|=1$, $j=1,2$, only if $\lambda=\frac{1}{2}$. Note that the damping of $|E_1^-|$ and $|E_2^-|$ for $\sigma=\frac{1}{2}$ in Figure 4, has previously been observed when the analogous least-squares scheme is used [33]. Furthermore, as for the CG scheme, the present method is only conditionally stable when $\sigma=0$.

Finally, for $kh=\pi$ (and $c \neq 0$) we have $|E_j^{\pm}| \neq 1$, $j=1,2$, while $|E_*|=1$ as shown in Figure 5. As for the finite-difference case examined in Section 2, the solution of the CG scheme exhibits a spurious elevation mode when $kh=\pi$, corresponding to stationary waves of length $2h$. It is quite interesting and important to note that such a spurious mode is not present in the discretization of the shallow-water equations using the DG method when the same linear approximation is used for both velocity and surface elevation fields.

5.2. *The case* $\mu=\lambda$ *and* $v=1-\lambda$ (DG2)

Equation (23) for $\varphi=\varphi_{j^+}$ and $\varphi_{(j+1)^-}$, respectively, still implies the pair of Equations (26) and (27), since $\mu=\lambda$. However, for (24) with $\psi=\psi_{j^+}$ and $\psi_{(j+1)^-}$ the choice $v=1-\lambda$ leads, respectively, to

$$\begin{aligned}
&\frac{h}{3}\eta_{j^+}^{n+1} + \frac{h}{6}\eta_{(j+1)^-}^{n+1} + \frac{\sigma}{2}H\Delta t(-2\lambda u_{j^-}^{n+1} + (2\lambda-1)u_{j^+}^{n+1} + u_{(j+1)^-}^{n+1}) \\
&\quad = \frac{h}{3}\eta_{j^+}^{n} + \frac{h}{6}\eta_{(j+1)^-}^{n} - \frac{(1-\sigma)}{2}H\Delta t(-2\lambda u_{j^-}^{n} + (2\lambda-1)u_{j^+}^{n} + u_{(j+1)^-}^{n}) \qquad (44)\\
&\frac{h}{6}\eta_{j^+}^{n+1} + \frac{h}{3}\eta_{(j+1)^-}^{n+1} + \frac{\sigma}{2}H\Delta t(-u_{j^+}^{n+1} + (2\lambda-1)u_{(j+1)^-}^{n+1} + 2(1-\lambda)u_{(j+1)^+}^{n+1}) \\
&\quad = \frac{h}{6}\eta_{j^+}^{n} + \frac{h}{3}\eta_{(j+1)^-}^{n} - \frac{(1-\sigma)}{2}H\Delta t(-u_{j^+}^{n} + (2\lambda-1)u_{(j+1)^-}^{n} + 2(1-\lambda)u_{(j+1)^+}^{n}) \qquad (45)
\end{aligned}$$

Periodic solutions of discrete system (26)–(27) and (44)–(45) corresponding to $u_{j\pm} = \tilde{u}_{\pm} e^{i(kx_{j\pm} + \omega t)}$ and $\eta_{j\pm} = \tilde{\eta}_{\pm} e^{i(kx_{j\pm} + \omega t)}$ are again sought. Substituting in (26)–(27) and (44)–(45), we obtain

$$\begin{pmatrix} 2\alpha & \alpha e^{ikh} & g\beta(1-2\lambda) & g\beta(e^{ikh}-2+2\lambda) \\ \alpha e^{-ikh} & 2\alpha & g\beta(2\lambda - e^{-ikh}) & g\beta(1-2\lambda) \\ H\beta(2\lambda-1) & H\beta(e^{ikh}-2\lambda) & 2\alpha & \alpha e^{ikh} \\ H\beta(2-2\lambda-e^{-ikh}) & H\beta(2\lambda-1) & \alpha e^{-ikh} & 2\alpha \end{pmatrix} \mathbf{X} = \mathbf{0} \tag{46}$$

where $\mathbf{X}^t = (\tilde{u}_+, \tilde{u}_-, \tilde{\eta}_+, \tilde{\eta}_-)$ and $\mathbf{0}^t = (0,0,0,0)$.

For a non-trivial solution $\mathbf{X}$ to exist, the determinant condition now implies

$$9\alpha^4 + 4gH\alpha^2\beta^2 C + 8g^2H^2\beta^4 D = 0 \tag{47}$$

with

$$C = 8 - 16\lambda + 16\lambda^2 + (1 - 16\lambda + 16\lambda^2)\cos kh + 4\lambda(\lambda-1)\cos^2 kh \tag{48}$$

$$D = 1 - 2\lambda + 2\lambda^2 - \cos kh + 2\lambda(1-\lambda)\cos^2 kh \tag{49}$$

Solving (47) for α^2 and using (30) we obtain the following pair of solutions for E:

$$E_j = \frac{1 \pm i(1-\sigma)cr_j}{1 \mp i\sigma cr_j}, \quad j = 3,4 \tag{50}$$

where

$$r_j = \sqrt{2C \mp 2\sqrt{C^2 - 18D}}, \quad j = 3,4 \tag{51}$$

with $2C \mp 2\sqrt{C^2 - 18D} \geqslant 0$ for all λ and kh.

In the limit as infinitesimal time step $\Delta t \to 0$ and for all σ, the discrete frequencies obtained from (50) asymptote to the real expressions

$$\omega_j = \pm \frac{\sqrt{gH}}{h} r_j, \quad j = 3,4 \tag{52}$$

and for infinitesimal mesh spacing we obtain

$$\omega_3 = \begin{cases} \pm\sqrt{gH}\,\mathrm{sgn}\left(\lambda - \frac{1}{2}\right)\left(\frac{6(2\lambda-1)}{h} - \frac{16\lambda^2 - 16\lambda + 1}{4(2\lambda-1)}k^2h + O(h^3)\right) \\ \qquad \text{if} \quad \lambda \neq \frac{1}{2} \\ \pm\sqrt{gH}\left(3k - \frac{5}{16}k^3h^2 + O(h^4)\right) \quad \text{if} \quad \lambda = \frac{1}{2} \end{cases} \tag{53}$$

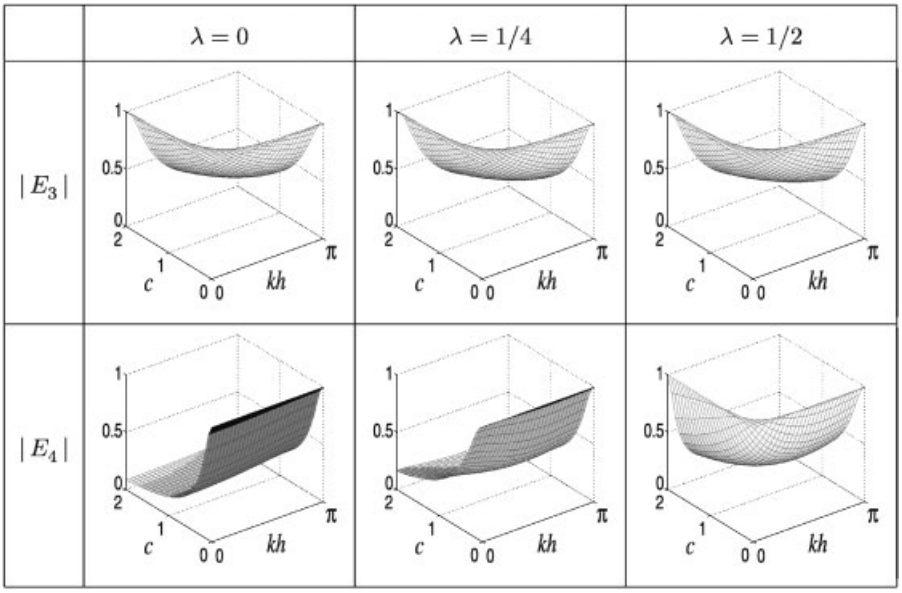

Figure 6. $|E_j|$, $j=3,4$, in the case $\sigma=1$ with $\lambda=0, \frac{1}{4}$ and $\frac{1}{2}$.

$$\omega_4 = \begin{cases} \pm\sqrt{gH}\left(k - \dfrac{24\lambda^2 - 24\lambda + 1}{1080(4\lambda^2 - 4\lambda + 1)}k^5h^4 + O(h^6)\right) & \text{if} \quad \lambda \neq \dfrac{1}{2} \\ \pm\sqrt{gH}\left(k + \dfrac{1}{48}k^3h^2 + O(h^4)\right) & \text{if} \quad \lambda = \dfrac{1}{2} \end{cases} \tag{54}$$

Note that only ω_4 coincides with the continuous solution obtained from (3) in the limit as mesh spacing $h \to 0$, while ω_3 corresponds to a spurious *propagating* mode from the DG scheme.

Equation (50) leads to

$$|E_j| = \sqrt{\frac{1 + ([1-\sigma]cr_j)^2}{1 + (\sigma cr_j)^2}}, \quad j = 3,4 \tag{55}$$

A necessary and sufficient condition for stability is that $|E_j| \leqslant 1$, $j=3,4$. For $\sigma=0$ the present method is only conditionally stable, and for $\sigma=\frac{1}{2}$ it is neutrally stable ($|E_j|=1$ for $j=3,4$) as for the CG case. Finally, for $\sigma=1$ the scheme is stable but the modes corresponding to (50) are damped as shown in Figure 6. The surprising behaviour of $|E_4|$ for $k=0$ in the cases $\lambda=0$ and $\frac{1}{4}$ is due to the presence of the term $6(2\lambda-1)/h$ in (53) when $\lambda \neq \frac{1}{2}$. Indeed, this term is independent of k and it leads to $\omega_3 \neq 0$, and hence $|E_4| \neq 1$, for $k=0$.

5.3. *The Riemann problem approach* (DG3)

We now assume that the averages $\langle . \rangle_\mu$ and $\langle . \rangle_v$ in (23) and (24) are chosen through the solution of the Riemann problem (see Reference [34, Section 4.5.2]) for system (1)–(2) written in the matrix form

$$\mathbf{w}_t + A\mathbf{w}_x = \mathbf{0} \quad \text{with} \quad A = \begin{pmatrix} 0 & H \\ g & 0 \end{pmatrix} \quad \text{and} \quad \mathbf{w} = (\eta, u) \tag{56}$$

Two waves are associated with the characteristic speeds $-\sqrt{gH}$ and $\sqrt{gH}$, the eigenvalues of matrix A, and the corresponding characteristic curves are defined by $x + \sqrt{gH}t = 0$ and $x - \sqrt{gH}t = 0$, respectively. The two waves separate the $x - t$ domain into three regions. In the region of interest, usually called the star region which lies between the two characteristic curves, the solutions of the Riemann problem for η and u involve arithmetic means and jumps of their initial data (see Reference [34, Section 4.5.2]).

We use the solutions for η and u in the star region to compute the fluxes at the cell interfaces. Hence, at time t^n, the weighted averages in (23) and (24) become

$$\langle \eta_j^n \rangle_\mu = \frac{1}{2}(\eta_{j^-}^n + \eta_{j^+}^n) + \frac{1}{2}\sqrt{\frac{H}{g}}(u_{j^-}^n - u_{j^+}^n) \tag{57}$$

$$\langle u_j^n \rangle_v = \frac{1}{2}(u_{j^-}^n + u_{j^+}^n) + \frac{1}{2}\sqrt{\frac{g}{H}}(\eta_{j^-}^n - \eta_{j^+}^n) \tag{58}$$

Note in (57) and (58), $\langle . \rangle_\mu$ and $\langle . \rangle_v$ are now independent of μ and v. The first term in the right hand sides of (57) and (58) is the arithmetic mean, corresponding to the choice $\mu = v = \frac{1}{2}$ in (23) and (24), while the second term, the jump, may be considered as an upwind term.

By following the same procedure as in Section 5.1, Equation (23) for $\varphi = \varphi_{j^+}$ and $\varphi = \varphi_{(j+1)^-}$ respectively, implies the pair of equations

$$\begin{aligned} &\frac{h}{3}u_{j^+}^{n+1} + \frac{h}{6}u_{(j+1)^-}^{n+1} + \frac{\sigma}{2}g\Delta t\left(-\eta_{j^-}^{n+1} + \eta_{(j+1)^-}^{n+1} - \sqrt{\frac{H}{g}}(u_{j^-}^{n+1} - u_{j^+}^{n+1})\right) \\ &= \frac{h}{3}u_{j^+}^{n} + \frac{h}{6}u_{(j+1)^-}^{n} - \frac{(1-\sigma)}{2}g\Delta t\left(-\eta_{j^-}^{n} + \eta_{(j+1)^-}^{n} - \sqrt{\frac{H}{g}}(u_{j^-}^{n} - u_{j^+}^{n})\right) \end{aligned} \tag{59}$$

$$\begin{aligned} &\frac{h}{6}u_{j^+}^{n+1} + \frac{h}{3}u_{(j+1)^-}^{n+1} + \frac{\sigma}{2}g\Delta t\left(-\eta_{j^+}^{n+1} + \eta_{(j+1)^+}^{n+1} + \sqrt{\frac{H}{g}}(u_{(j+1)^-}^{n+1} - u_{(j+1)^+}^{n+1})\right) \\ &= \frac{h}{6}u_{j^+}^{n} + \frac{h}{3}u_{(j+1)^-}^{n} - \frac{(1-\sigma)}{2}g\Delta t\left(-\eta_{j^+}^{n} + \eta_{(j+1)^+}^{n} + \sqrt{\frac{H}{g}}(u_{(j+1)^-}^{n} - u_{(j+1)^+}^{n})\right) \end{aligned} \tag{60}$$

Similarly, for (24) with $\psi=\psi_{j^+}$ and $\psi=\psi_{(j+1)^-}$, respectively, we obtain

$$\frac{h}{3}\eta_{j^+}^{n+1}+\frac{h}{6}\eta_{(j+1)^-}^{n+1}+\frac{\sigma}{2}H\Delta t\left(-u_{j^-}^{n+1}+u_{(j+1)^-}^{n+1}-\sqrt{\frac{g}{H}}(\eta_{j^-}^{n+1}-\eta_{j^+}^{n+1})\right)$$
$$=\frac{h}{3}\eta_{j^+}^{n}+\frac{h}{6}\eta_{(j+1)^-}^{n}-\frac{(1-\sigma)}{2}H\Delta t\left(-u_{j^-}^{n}+u_{(j+1)^-}^{n}-\sqrt{\frac{g}{H}}(\eta_{j^-}^{n}-\eta_{j^+}^{n})\right) \quad (61)$$

$$\frac{h}{6}\eta_{j^+}^{n+1}+\frac{h}{3}\eta_{(j+1)^-}^{n+1}+\frac{\sigma}{2}H\Delta t\left(-u_{j^+}^{n+1}+u_{(j+1)^+}^{n+1}+\sqrt{\frac{g}{H}}(\eta_{(j+1)^-}^{n+1}-\eta_{(j+1)^+}^{n+1})\right)$$
$$=\frac{h}{6}\eta_{j^+}^{n}+\frac{h}{3}\eta_{(j+1)^-}^{n}-\frac{(1-\sigma)}{2}H\Delta t\left(-u_{j^+}^{n}+u_{(j+1)^+}^{n}+\sqrt{\frac{g}{H}}(\eta_{(j+1)^-}^{n}-\eta_{(j+1)^+}^{n})\right) \quad (62)$$

Periodic solutions are again substituted in the discrete system (59)–(62) and this leads to

$$\begin{pmatrix} 2\alpha+\sqrt{gH}\beta & \alpha e^{ikh}-\sqrt{gH}\beta & 0 & g\beta(e^{ikh}-1) \\ \alpha e^{-ikh}-\sqrt{gH}\beta & 2\alpha+\sqrt{gH}\beta & g\beta(1-e^{-ikh}) & 0 \\ 0 & H\beta(e^{ikh}-1) & 2\alpha+\sqrt{gH}\beta & \alpha e^{ikh}-\sqrt{gH}\beta \\ H\beta(1-e^{-ikh}) & 0 & \alpha e^{-ikh}-\sqrt{gH}\beta & 2\alpha+\sqrt{gH}\beta \end{pmatrix}\mathbf{X}=\mathbf{0} \quad (63)$$

where $\mathbf{X}^t=(\tilde{u}_+,\tilde{u}_-,\tilde{\eta}_+,\tilde{\eta}_-)$ and $\mathbf{0}^t=(0,0,0,0)$.

For a non-trivial solution $\mathbf{X}$ to exist, the determinant condition implies

$$9\rho^4+12(\cos kh+2)\rho^3\beta+4(\cos kh+8)\rho^2\beta^2-8(\cos kh-1)\rho\beta^3+8(1-\cos kh)\beta^4=0 \quad (64)$$

where $\rho=\alpha/\sqrt{gH}$. After some long and tedious algebra (64) is rewritten as

$$(3\rho^2+2(e^{ikh}+2)\rho\beta-2(e^{ikh}-1)\beta^2)$$
$$\times(3\rho^2+2(e^{-ikh}+2)\rho\beta-2(e^{-ikh}-1)\beta^2)=0 \quad (65)$$

Solving (65) for α^2 and using (30) we obtain the following pair of solutions for E

$$E_j^{\pm}=\frac{1+(1-\sigma)cr_j^{\pm}}{1-\sigma cr_j^{\pm}},\quad j=5,6 \quad (66)$$

where

$$r_5^{\pm}=-(e^{ikh}+2)\pm\sqrt{(e^{ikh}+2)^2+6(e^{ikh}-1)}\equiv r_5^{R\pm}+ir_5^{I\pm} \quad (67)$$

$$r_6^{\pm}=-(e^{-ikh}+2)\pm\sqrt{(e^{-ikh}+2)^2+6(e^{-ikh}-1)}\equiv r_6^{R\pm}+ir_6^{I\pm} \quad (68)$$

with $r_j^{R\pm}$ and $r_j^{I\pm}$ being, respectively, the real and imaginary parts of $r_j^{\pm}$, $j=5,6$, with $r_6^{R\pm}=r_5^{R\pm}$ and $r_6^{I\pm}=-r_5^{I\pm}$.

In the limit as infinitesimal time step $\Delta t \to 0$ and for all σ, the discrete frequencies obtained from (66) asymptote to the complex expressions

$$\omega_j^{\pm} = \frac{\sqrt{gH}}{h}\,(r_j^{\mathrm{I}\pm} - \mathrm{i} r_j^{\mathrm{R}\pm}), \quad j = 5, 6 \tag{69}$$

and for infinitesimal mesh spacing we obtain

$$\omega_5^{+} = \sqrt{gH}\left(k + \frac{\mathrm{i}}{72}\,k^4 h^3 + O(h^4)\right) \tag{70}$$

$$\omega_5^{-} = \sqrt{gH}\left(\frac{6\mathrm{i}}{h} - 3k - \mathrm{i}k^2 h + \frac{1}{3}\,k^3 h^2 + \frac{5\mathrm{i}}{72}\,k^4 h^3 + O(h^4)\right) \tag{71}$$

$$\omega_6^{+} = \sqrt{gH}\left(-k + \frac{\mathrm{i}}{72}\,k^4 h^3 + O(h^4)\right) \tag{72}$$

$$\omega_6^{-} = \sqrt{gH}\left(\frac{6\mathrm{i}}{h} + 3k - \mathrm{i}k^2 h - \frac{1}{3}\,k^3 h^2 + \frac{5\mathrm{i}}{72}\,k^4 h^3 + O(h^4)\right) \tag{73}$$

Note that ω_5^{+} and ω_6^{+} in (70) and (72), respectively, coincide with the continuous solution obtained from (3) in the limit as mesh spacing $h \to 0$, while ω_5^{-} and ω_6^{-} in (71) and (73), respectively, correspond to spurious *propagating* modes from the DG scheme.

Equation (66) leads to

$$|E_j^{\pm}| = \sqrt{\frac{(1 + [1-\sigma]cr_j^{\mathrm{R}\pm})^2 + ([1-\sigma]cr_j^{\mathrm{I}\pm})^2}{(1 - \sigma cr_j^{\mathrm{R}\pm})^2 + (\sigma cr_j^{\mathrm{I}\pm})^2}} \quad j = 5, 6 \tag{74}$$

A necessary and sufficient condition for stability is then obtained from (74):

$$|E_j^{\pm}| \leqslant 1 \iff c(2\sigma - 1)((r_j^{\mathrm{R}\pm})^2 + (r_j^{\mathrm{I}\pm})^2) \geqslant 2r_j^{\mathrm{R}\pm}, \ j = 5, 6 \tag{75}$$

Some calculations show that $r_j^{\mathrm{R}\pm} \leqslant 0$, $j = 5, 6$, for all kh. Hence, at least for $\sigma \geqslant \frac{1}{2}$ the scheme is unconditionally stable. For $\sigma = \frac{1}{2}$, the scheme is neutrally stable if $r_j^{\mathrm{R}\pm} = 0$, and this only happens for $kh = 0(2\pi)$ in r_j^{+}, $j = 5, 6$. Note the term $6i/h$ in (71) and (73) implies $|E_5^{-}| \neq 1$ and $|E_6^{-}| \neq 1$ for $kh = 0$ in both cases $\sigma = \frac{1}{2}$ and 1. In conclusion, when the scheme is stable the modes corresponding to (66) are always damped, as shown in Figure 7.

6. NUMERICAL RESULTS

In the previous section, it has been observed that in the respective DG schemes, the spurious frequencies ω_1 and ω_2 in (38) for $\lambda \neq \frac{1}{2}$ and (39) for $\lambda = \frac{1}{2}$, respectively, ω_3 in (53), and ω_5^{-} and ω_6^{-} in (71) and (73), respectively, do not agree with the continuous solution as mesh spacing $h \to 0$. In order to evaluate the impact of the spurious modes on the quality of the numerical solution a simulation test is performed. We examine the propagation and dispersion of gravity waves in a one-dimensional enclosed domain of length $L = 10\,000$ km. Equations

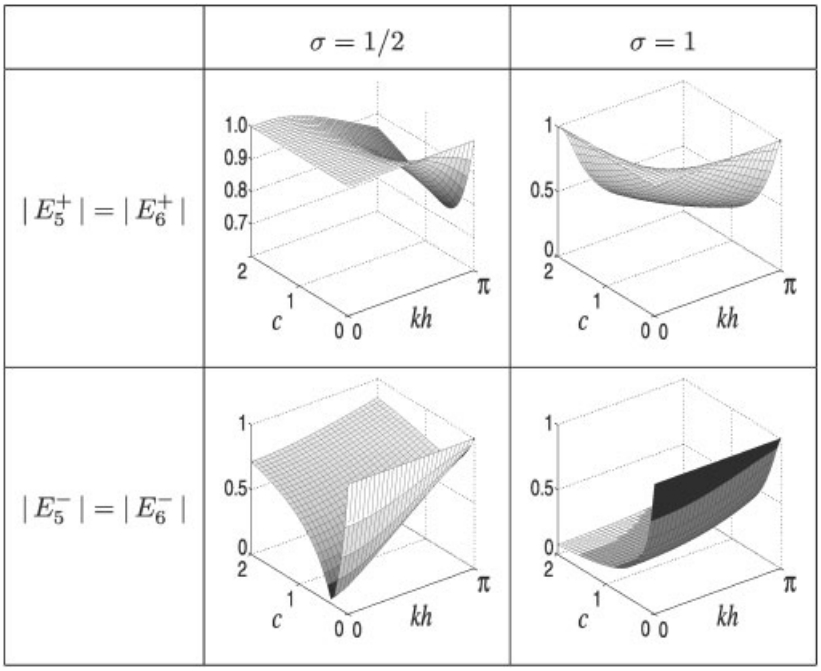

Figure 7. $|E_j^{\pm}|$, $j = 5, 6$, in the cases $\sigma = \frac{1}{2}$ and 1.

(1) and (2) are solved with parameters g and H set to result in a phase speed for gravity waves of $\sqrt{gH} = 100\ \mathrm{m\,s^{-1}}$. A Gaussian distribution, centered at x_0, is prescribed at initial time and the initial velocity field is taken to be zero, i.e.

$$\eta(x, 0) = \mathrm{e}^{-\left(\frac{x - x_0}{\delta}\right)^2} \tag{76}$$

$$u(x, 0) = 0 \tag{77}$$

with $x_0 = 5000\,\mathrm{km}$. The distance h between two velocity nodes is taken to be 10 km, and the parameter δ is chosen to be 50 km so that the e-folding radius of the initial Gaussian (the distance x from x_0 for which $\eta(x, 0) = e^{-1}$) is resolved by 5 nodes.

In the first simulation, the time step is chosen to be 0.1 s, and thus the gravitational Courant number is $C_g = \sqrt{gH}\,\Delta t/h = 10^{-3}$. With such a small value for C_g, the numerical solution should be expected to approximate the analytical one reasonably well. Furthermore, the use of a forward Euler ($\sigma = 0$) and a Crank–Nicolson ($\sigma = \frac{1}{2}$) time stepping schemes yield essentially the same results. The evolution of the surface elevation is shown in Figure 8 after 15 000 s of simulation for the DG scheme and the results are compared with those of the CG case. Note only half of the domain is shown since all the numerical results presented in this section are symmetric with respect to $x_0 = 5000\,\mathrm{km}$.

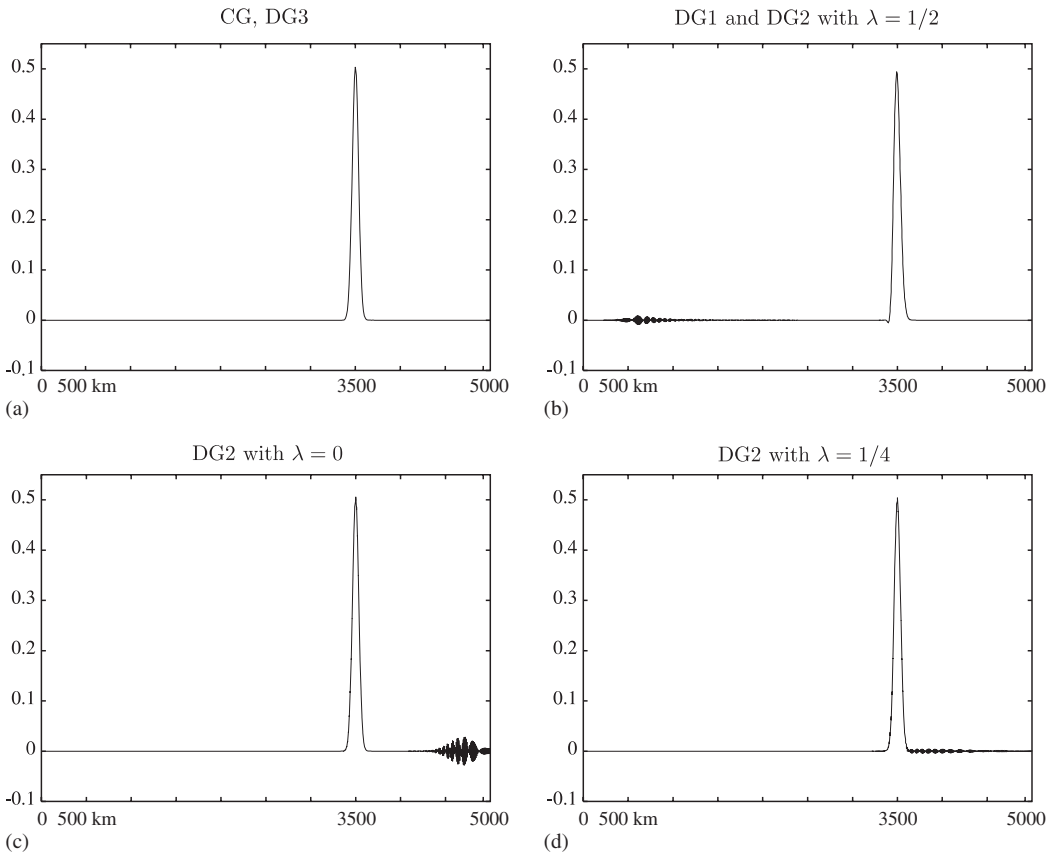

Figure 8. The surface-elevation after 15 000 s of propagation with $\Delta t = 0.1$ s in the explicit case ($\sigma = 0$) for the CG and DG schemes: (a) CG, DG3; (b) DG1 and DG2 with $\lambda = \frac{1}{2}$, (c) DG2 with $\lambda = 0$; and (d) DG2 with $\lambda = \frac{1}{4}$.

The initial Gaussian has an amplitude equal to 1. Shortly after the beginning of the simulation the Gaussian is split into two Gaussians, each having an amplitude equal to 0.5 and travelling with an opposite phase speed of $\pm\sqrt{gH}$. In Figure 8, the DG scheme reproduces quite well such behaviour, as does the CG scheme. However, we also notice for the DG1 and DG2 schemes, the presence and the propagation of spurious solutions identified in Section 5. Indeed, (39) and (53), corresponding to the DG1 or DG2 scheme for $\lambda = \frac{1}{2}$, yield numerical modes having phase speeds $\pm 3\sqrt{gH}$. In Figure 8(b), as the Gaussian propagates over 1500 km, the spurious DG solution propagates exactly and precisely over 4500 km. The spurious modes corresponding to the DG2 scheme for $\lambda = 0$ and $\frac{1}{4}$ are evident in Figures 8(c) and (d), respectively. Finally, the DG3 solution coincide with the CG solution. Note that the amplitude of the spurious modes, when they exist, is enhanced by employing a longer time step and reduced by using a smaller one.

In the second simulation the backward Euler scheme is employed ($\sigma = 0$) which allows the use of larger times steps. For $\Delta t = 1$s, the DG2 results with $\lambda = 0$ and $\frac{1}{4}$ now coincide

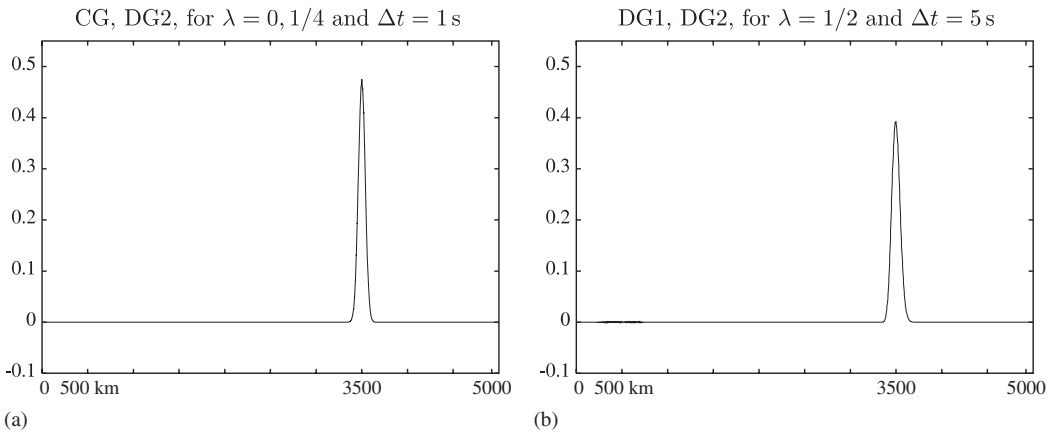

Figure 9. The surface-elevation after 15 000 s of propagation in the implicit case ($\sigma = 1$) for the CG and DG schemes: (a) CG, DG2, for $\lambda = 0, \frac{1}{4}$ and $\Delta t = 1$ s; and (b) DG1, DG2, for $\lambda = \frac{1}{2}$ and $\Delta t = 5$ s.

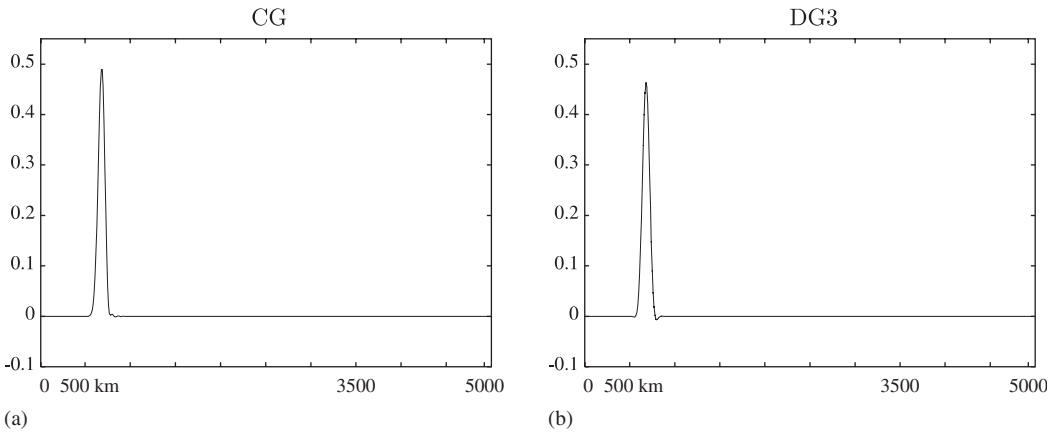

Figure 10. The surface-elevation after 12 h of propagation with $\Delta t = 20$ s in the Crank–Nicolson case ($\sigma = \frac{1}{2}$) for the CG and DG3 schemes: (a) CG; and (b) DG3.

with the CG solution, as shown in Figure 9(a), implying the spurious modes (but also the solution) have been damped. The DG3 result (not shown) presents a similar behaviour, but the damping of the Gaussian is slightly more pronounced. However, when $\lambda = \frac{1}{2}$, the spurious mode corresponding to the DG1 or DG2 schemes is still visible in Figure 9(b), in spite of using a much longer time step ($\Delta t = 5$ s) which contributes to severely damp the Gaussian.

The last simulation is performed up to 12 h using the Crank–Nicolson scheme ($\sigma = \frac{1}{2}$) and the time step is chosen to be 20 s. As shown in Figure 10 the DG3 solution is noticeably damped compared to the Galerkin one. This result illustrates the stability/dispersion plots obtained in Figure 7.

7. CONCLUDING REMARKS

This appears to be the first study of the dispersion relation and spurious mode behavior for finite-element solutions of the 1-D linearized shallow-water equations based on the DG approach. There are a number of variants of DG methods that have been proposed recently in the literature in both the shallow-water context and also for other applications classes. Indeed, the idea of using discontinuous approximations across element boundaries with weak enforcement of continuity conditions is hardly new. This approach has not been popular largely because of questions concerning the increased number of degrees of freedom and consequent implications concerning efficiency. Nevertheless, the approach merits study and since local conservation or other special properties such as adaptive meshing can be easily enforced, the schemes are of interest.

Here we construct the dispersion relation of some basic DG mixed schemes using piecewise-linear basis functions, with the respective velocity and elevation variables located at the same nodal positions. We study the folding behaviour for spurious modes as well as the phase behaviour and dissipative effects. The behaviour is compared analytically and graphically with that of the CG mixed formulation to illustrate the main points of interest. These results can also be compared with those in Reference [33] for the least squares mixed formulation which is more dissipative. A numerical test case, concerning the propagation of gravity waves, illustrates the theoretical results obtained for the spurious solutions of the DG scheme, and in particular their phase speeds. A spurious propagating mode traveling at three times the gravity mode is seen (Figure 8(b)).

It is important to note that spurious stationary surface-elevation modes have not been found in the DG schemes examined here, contrary to the corresponding CG case. However, spurious propagating modes have been identified in all the present DG formulations. The origin of these modes is linked with the increased number of the discrete variables compared to the CG scheme (twice in 1-D), leading to additional discrete frequencies which are usually spurious. The nature of those propagating modes has not been investigated here, but it strongly depends on the flux formulation at the element interfaces and the temporal scheme. This is why time-integration methods other than those examined here should be investigated in future works.

We close by noting that there are many ways to express DG formulations including adding least squares terms as interface penalties and a dispersion analysis of such schemes should be carried out numerically before they are implemented or advocated for applications. Likewise the effects of additional terms such as Coriolis that are not included in the present construction should be studied (see Reference [33] for related studies). An explicit algebraic construction of the form used here will be prohibitive in higher dimensions or with more complex equations but symbolic manipulation or a numerical eigen-analysis treatment is then still possible.

ACKNOWLEDGEMENTS

This work is supported by grants to D.Y.L from the Natural Sciences and Engineering Research Council (NSERC), and FQRNT (Fonds Québécois de la Recherche sur la Nature et les Technologies). We gratefully acknowledge Dr Serge Prudhomme and Prof Vincent Legat and Jean-François Remacle for their suggestions and advice.

REFERENCES

1. Lynch DR, Gray WG. A wave-equation model for finite-element tidal computations. *Computers and Fluids* 1979; **7**:207–228.
2. Carey GF (ed.). *Finite Element Modeling of Environmental Problems*. Wiley: UK, 1995.
3. Dumas E, Le Provost C, Poncet A. Feasibility of finite-element methods for oceanic general circulation modeling. *4th International Conference on Finite Element in Water Resources*, vol. 5. Springer: New York, 1982; 43–55.
4. Fix GJ. Finite element models for ocean circulation problems. *SIAM Journal on Applied Mathematics* 1975; **29**:371–387.
5. Hua BL, Thomasset F. A noise-free finite-element scheme for the two-layer shallow-water equations. *Tellus* 1984; **36A**:157–165.
6. Iskandarani M, Haidvogel D, Boyd J. A staggered spectral finite-element model for the shallow-water equations. *International Journal for Numerical Methods in Fluids* 1995; **20**:393–414.
7. Le Provost C, Vincent P. Finite element for modeling ocean tides. In *Tidal Hydrodynamics*, Parker B (ed.). Wiley: New York, 1991; 41–60.
8. Le Roux DY, Staniforth A, Lin CA. Finite elements for shallow-water equation ocean models. *Monthly Weather Review* 1998; **126**:1931–1951.
9. Lynch DR, Werner FE. Three dimensional hydrodynamics on finite elements. Part 2: nonlinear time stepping model. *International Journal for Numerical Methods in Fluids* 1991; **12**:507–533.
10. Walters RA, Cheng RT. Accuracy of an estuarine hydrodynamic model using smooth elements. *Water Resources Research* 1980; **16**(1):187–195.
11. Danilov S, Kivman G, Schröter J. A finite-element ocean model: principles and evaluation. *Ocean Modelling* 2004; **6**:125–150.
12. Foreman MGG, Walters RA, Henry RF, Keller CP, Dolling AG. A tidal model for eastern Juan de Fuca Strait and the southern Strait of Georgia. *Journal of Geophysical Research* 1995; **100**:721–740.
13. Le Roux DY, Lin CA, Staniforth A. A semi-implicit semi-Lagrangian finite-element shallow-water ocean model. *Monthly Weather Review* 2000; **128**:1384–1401.
14. Nechaev D, Schröter J, Yaremchuk M. A diagnostic stabilized finite-element ocean circulation model. *Ocean Modelling* 2003; **5**:37–63.
15. Walters RA. A three-dimensional finite-element model for coastal and estuarine circulation. *Continental Shelf Research* 1992; **12**:83–102.
16. Walters RA, Barragy EJ. Comparison of h and p finite-element approximations of the shallow-water equations. *International Journal for Numerical Methods in Fluids* 1997; **24**:61–79.
17. Walters RA, Casulli V. A robust, finite-element model for hydrostatic surface water flows. *Communications in Numerical Methods in Engineering* 1998; **14**:931–940.
18. Bercovier M, Pironneau O. Error estimates for the finite-element method solution of the Stokes problem in the primitive variables. *Numerical Mathematik* 1979; **33**:211–224.
19. Brezzi F. On the existence, uniqueness and approximation of saddle point problems arising from Lagrangian multipliers. *R.A.I.R.O.* 1974; **8**:129–151.
20. Brezzi F, Fortin M. *Mixed and Hybrid Finite Element Methods*. Springer Series in Computational Mathematics, vol. 15. Springer: Berlin, 1991.
21. Girault V, Raviart PA. *Finite Element Methods for Navier–Stokes Equations*. Springer Series in Computational Mathematics, vol. 5. Springer: Berlin, 1986.
22. Temam R. *Navier–Stokes Problems*. North-Holland: Amsterdam, 1977.
23. Walters RA, Carey GF. Analysis of spurious oscillation modes for the shallow-water and Navier–Stokes equations. *Computers and Fluids* 1983; **11**:51–68.
24. Myers PG, Weaver AJ. A diagnostic barotropic finite-element ocean circulation model. *Journal of Atmospheric and Oceanic Technology* 1995; **12**:511–526.
25. Aizinger V, Dawson C. A discontinuous Galerkin method for two-dimensional flow and transport in shallow water. *Advances in Water Resources* 2002; **25**:67–84.
26. Arnold DN, Brezzi F, Cockburn B, Marini LD. Unified analysis of discontinuous Galerkin methods for elliptic problems. *SIAM Journal on Numerical Analysis* 2002; **39**:1749–1779.
27. Cockburn B, Karniadakis E, Shu CW (eds). *Discontinuous Galerkin Methods—Theory, Computation and Applications*. Lectures Notes in Computational Science and Engineering, vol. 11. Springer: Berlin, 2000.
28. Dawson C, Proft J. Discontinuous/continuous Galerkin methods for coupling the primitive and wave continuity equations of shallow water. *TICAM Report 03-02*, ICES, The University of Texas at Austin, Austin, Texas, 2003.
29. Schwanenberg D, Köngeter J. A discontinuous Galerkin method for the shallow-water equations with source terms. In *Discontinuous Galerkin Methods—Theory, Computation and Applications*, Cockburn B, Karniadakis E, Shu CW (eds), Lectures Notes in Computational Science and Engineering, vol. 11. Springer: Berlin, 2000; 419–424.

30. LeBlond PH, Mysak LA. *Waves in the Ocean*. Elsevier: Amsterdam, 1978.
31. Robert A. The integration of a spectral model of the atmosphere by the implicit method. *Proceedings of the WMO/IUGG Symposium on NWP*, Tokyo, Japan Meteorological Agency, vol. VII, 1969; 19–24.
32. Robert A, Henderson J, Turnbull C. An implicit time integration scheme for baroclinic models of the atmosphere. *Monthly Weather Review* 1972; **100**:329–335.
33. Le Roux DY, Carey GF. Dispersion analysis of the least-squares finite-element shallow-water system. *International Journal for Numerical Methods in Fluids* 2003; **42**:607–622.
34. Toro EF. *Shock-Capturing Methods for Free-Surface Shallow Flows*. Wiley: New York, 2001.

